Wasteless Synthesis and Properties of Highly Dispersed MgAl$_2$O$_4$ Based on Product of Thermal Activation of Gibbsite

Aleksey V. Zhuzhgov *[ID], Vasily Y. Kruglyakov, Tatyana S. Glazneva [ID], Evgeny A. Suprun and Lyubov A. Isupova

Boreskov Institute of Catalysis, Lavrentieva Ave. 5, 630090 Novosibirsk, Russia; krugl@catalysis.ru (V.Y.K.); glazn@catalysis.ru (T.S.G.); suprun@catalysis.ru (E.A.S.); isupova@catalysis.ru (L.A.I.)

* Correspondence: zhuzhgov@catalysis.ru

Abstract: The study showed that the interaction of the product of centrifugal thermal activation of gibbsite with an aqueous solution of magnesium nitrate at a cationic ratio Mg:Al = 1:2 leads to the formation of mixed double hydroxides both under hydrothermal treatment at 150 °C and at room temperature. The subsequent thermal treatment at 550 °C of the product of mild interaction leads to ~90% alumina-magnesia spinel and ~10% MgO, while the treatment of the hydrothermal interaction product leads to ~100% spinel with the stoichiometric composition MgAl$_2$O$_4$. The obtained spinel samples possess a high specific surface area (above 100 m^2/g) and a hierarchical pore structure formed by the micron-level particles of different sizes (1–2 and 10–20 μm) consisting of ~70 nm crystallites with ~3 nm pores; the samples differ mostly in the total volume and quantitative ratio of the pores. The samples have Lewis acid sites of moderate strength on the surface, the amount of which is much lower to how it is when compared with a sample prepared by precipitation in that they also differ by quantity from each other as well (503 μmol/g for stoichiometric spinel and 304 μmol/g for sample with admixture of MgO). As the calcination temperature is raised to 850 °C, the acidity decreases—only weak Lewis acid sites are observed, the amount of which is also higher for stoichiometric spinel (161 and 39 μmol/g, respectively). The method proposed for the synthesis of alumina-magnesia systems provides a high dispersion and a much lower surface acidity for the oxides; in addition, it minimizes or completely excludes wash water, in distinction to the precipitation method.

Keywords: MgAl$_2$O$_4$; wasteless synthesis; texture; surface acidity

1. Introduction

Magnesium aluminate MgAl$_2$O$_4$, with its spinel structure, is of considerable interest for application in catalysis due to its high thermal stability and its low acidity on its surface compared with the low-temperature modifications of aluminum oxides, which is very important in the development and improvement of the catalysts for the processing of hydrocarbon hydrogenation and dehydrogenation as well as the catalysts for high-temperature oxidation reactions [1–8]. For example, it was found that an increase in the Mg fraction in the MgAl-O oxide system synthesized by precipitation (according to the sol-gel technology) decreases both the strength and concentration of acid sites on the surface, thus changing the properties of supported platinum [4]. The application of supported Pt/MgAl-O catalysts in the dehydrogenation of n-decane ensures the 90% selectivity for the formation of n-decenes, a decrease in the yield of products from cracking and skeletal isomerization of decane, and a decrease in the content of diene hydrocarbons [4]. A similar decrease in the surface acidity was observed also when Al$_2$O$_3$ was doped by magnesium cations using incipient wetness impregnation with a magnesium nitrate solution. IR spectroscopy of adsorbed CO molecules and pyridine was used to demonstrate that the general trend is a decrease in the concentration and strength of Lewis acid sites (LAS) and Broensted acid (proton) sites with an increasing content of Mg^{2+} cations in the alumina matrix, which

was favorable for the steam conversion of ethanol and glycerol [8]. Currently, mixed oxide systems are also being used; for example, NiO-MgO-Al$_2$O$_3$, in which (Ni + Mg)Al $\geq$ 2, which exhibits a high activity and stability as a catalyst for the methanation of CO$_2$ into useful fuels and valuable chemical products [9–11].

The literature considers various synthesis methods of magnesium aluminates as well as other A^{2+}B$^{3+}_2$O$^{2-}_4$ spinels, their advantages and drawbacks. The main advantage and drawback of the precipitation from solutions are the high values of specific surface areas of oxides and, consequently, the large consumption of reagents and the formation of wastes that should be utilized [5–8,12–15].

The mechanochemical method consists of a preliminary mechanical activation of the initial mixtures of hydroxides and/or oxides, which makes it possible to decrease the calcination temperature as compared with the ceramic method and to obtain dispersed materials with the specified properties [16–20]. However, this method is not widely used due to an absence of the appropriate industrial equipment.

An interesting approach to the synthesis of magnesium aluminate is the interaction of solid and liquid reagents. For example, in [21], well crystallized magnesium aluminate particles were obtained by treatment of a mixture of gibbsite and magnesium nitrate solution under harsh (450 °C) hydrothermal conditions.

Methods of thermal activation of gibbsite under conditions of rapid heating (1–10 s), leading to the formation of amorphous aluminum oxide-hydroxide, have received a wide practical application in the production of supports, catalysts, desiccants, and other functional materials [22–24]. This product is characterized by a high specific surface (>200 m^2/g) and increased chemical activity with respect to electrolytes, which leads to a significant increase in solubility in acids and alkalis compared to the original gibbsite [23–27], which makes it possible to prepare alumina carriers and adsorbents on its basis with various structural modifications without precipitation steps [23,25,27–30].

In [31], we have demonstrated that the product of centrifugal thermal activation (CTA) of gibbsite can be used to obtain stoichiometric alumina-magnesia spinel MgAl$_2$O$_4$ with a high value of specific surface area by holding the thermal activation product in magnesium nitrate solutions under hydrothermal conditions. In comparison with the conventional ceramic method, this makes it possible to decrease the calcination temperature and obtain a highly dispersed product, while in comparison with the precipitation method, it can be used to substantially decrease the amount of initial reagents and the number of technological steps, as well as to minimize or completely exclude the formation of wastewater and harmful nitrogen oxides (NO$_x$) in off-gases during the thermal treatment steps. As a result, the proposed method becomes quite attractive for use in various applications, particularly for the synthesis of MgAl$_2$O$_4$ supports and catalysts. It is known that the preparation method and conditions largely determine the texture and surface properties of oxides, which will ultimately affect their catalytic properties [8,25,27,28].

Therefore, the aim of the work was to synthesize magnesium aluminates via interactions of the product of centrifugal thermal activation of gibbsite with a magnesium nitrate solution at different conditions—under mild (room temperature) and hydrothermal treatment conditions—to study their physical and chemical properties: phase composition, textural features, microcrystal morphology, as well as acidic properties on the surface.

2. Experimental

2.1. Synthesis of Samples

Gibbsite GD 000 (Specs. 1711-99-039-2000) produced at the Achinsk Alumina Refinery served as the initial feedstock to obtain the product of centrifugal thermal activation of gibbsite IC-02-76 (Specs. 2175-040-03533913-2007). The content of impurities in the original gibbsite was as follows (wt.%): Fe = 0.002, Na = 0.11, K = 0.033, and Si = 0.014. The specific surface area of the original gibbsite powder did not exceed 1 m^2/g. Weight losses upon calcination at 850 °C were equal to 34 wt.%. Magnesium nitrate hexahydrate

$Mg(NO_3)_2 \cdot 6H_2O$ (analytically pure, Chemical Elements Ukraine LLC) was used as the initial Mg-containing feedstock.

Thermal activation of gibbsite was carried out in a drum-type centrifugal flash reactor (CEFLAR^{TM}) at a temperature of electric heaters 540 ± 5 °C, a drum rotation speed 60 rpm, and a flow rate of the initial powder 50 kg/h. Weight losses during calcination of the obtained product of centrifugal thermal activation at 850 °C were ca. 12.5 wt.%. The CTA product was then ground in a ball mill for 6 h to obtain a powder with the mean particle size of ca. 30–40 µm.

To synthesize the magnesium aluminate ($MgAl_2O_4$) samples, a preliminarily prepared magnesium nitrate solution was supplemented with the CTA product of gibbsite, so that the cationic ratio in suspension corresponded to 1:2. A suspension with the initial pH value of ca. 5.0 was stirred at a rate of 120 rpm for 4 h at ambient/normal and high pressures.

High pressure treatment was carried out in an autoclave by Top Industrie (France), providing hydrothermal treatment up to a temperature of 250 °C and a pressure of 200 bar. The autoclave is equipped with a magnetic stirrer with a maximum speed of 1500 rpm and a 350 mL stainless steel reactor (beaker). The control and regulation thermocouple, as well as the pressure transducer, are in the reaction medium during the experiments.

Gels formed via the interaction were dried at 110 °C for 12 h to obtain a xerogel, which was subjected to thermal treatment in a muffle furnace in air at 550 or 850 °C for 4 h. The samples were denoted as Mg-Al(1)-T and Mg-Al(2)-T, respectively, where 1 indicates treatment under normal conditions, 2 is hydrothermal treatment, and T is the calcination temperature (°C) of the sample.

2.2. Characterization of Samples

X-ray diffraction (XRD) analysis was carried out on a D-500 (Siemens, Germany, Munich) diffractometer using CuK_{α} radiation and a graphite reflected-beam monochromator. Diffraction patterns of the samples were obtained by scanning over the angular region $2\theta = 10$–$70\,°$ with a 0.05° step and a signal accumulation time of 3 s. Phases were identified by comparing the experimental diffraction patterns with the patterns from ICDD and PDF 2 databases.

Thermal analysis (TA) of the hydration products was performed on a synchronous thermal analyzer STA 449 C Jupiter (NETZSCH, Selb, Germany) over a temperature range from 20 to 850–1200 °C at a heating rate of 10 °C/min in air using ca. 30 mg samples.

The morphology of the surface layer of the calcined samples was examined on a scanning electron microscope Regulus SU8230 (Hitachi, Tokyo, Japan) with a probe electron energy 20–25 keV. The microscope was equipped with energy-dispersive X-ray spectrometers INCA Energy-350 and ULTIM MAX 100 (Oxford Instruments, Abingdon, UK), respectively, which allowed the determination of the elemental composition of samples in a layer up to 5 µm.

Textural characteristics were obtained using low-temperature nitrogen desorption at 77 K on an automated Quadrasorb-EVO Quantachrome (USA) instrument. The samples were studied as powders after their preliminary evacuation at 200 °C for 2 h. The techniques used for measuring and calculating the textural parameters complied with ASTM D3663, ASTM D4820, ASTM D1993, and UOP425-86 standards.

Mercury porosimetry studies were carried out on an AutoPore IV (Micromeritics, Norcross, GA, USA) porosimeter. As a result of measurements, mercury intrusion curves were obtained at a pressure of 0.1–4000 bar, which were used to calculate the apparent density of the material, its pore size distribution and its specific surface area. The measurement technique complied with ASTM D4284-03 (a method for measuring the effective pore size distribution for catalysts by the intrusion of mercury) and ASTM D4404-84 (2004) (a method for measuring the volume and pore size distribution in soils by mercury intrusion).

Chemical composition of the synthesized samples was identified by inductively coupled plasma atomic emission spectroscopy on an OPTIMA 4300 DV (Perkin Elmer, Waltham, MA, USA) instrument.

Acidic properties of the surface were studied by low-temperature Fourier transform infrared spectroscopy (FTIR) of adsorbed carbon monoxide. The samples were pressed into pellets with the size of 1×2 cm^2 and a total weight of 40–50 mg. The pellet was placed in an IR cuvette and calcined in vacuum for two hours at 500 °C and a residual gas pressure of ~10^{-4} Torr. The adsorption of CO was performed at −196 °C (77 K) and a CO pressure from 0.1 to 10 Torr. IR spectra were recorded on a Tracer-100 IR spectrometer in the region of 400–6000 cm^{-1} with a resolution of 4 cm^{-1} and a signal accumulation from 200 scans. The spectra on the absorption scale were normalized to the optical thickness of pellets. IR spectra were analyzed by decomposition of absorption bands into individual Gaussians. The strength of Lewis acid sites was estimated from the adsorption heats of carbon monoxide by the formula [32]:

$$Q_{co} \text{ [kJ/mol]} = 0.5 \times (\nu_{co} - 2143 \text{ cm}^{-1}) + 10.5 \tag{1}$$

where: ν_{co} (cm^{-1}) is the vibration frequency of CO adsorbed on LAS, and 2143 cm^{-1} corresponds to CO vibrations in the gas phase. The concentration of LAS was found from integrated intensities of the corresponding absorption bands of adsorbed carbon monoxide by the equation [18,19]:

$$C_s = (A/A_0 \times p) \times 10^{-3} \tag{2}$$

where: C_s (μmol/g) is the concentration of sites on the surface; A (cm^{-1}) is the apparent integrated absorption; A_0 is the integrated intensity of the absorption band; and p (mg) is the catalyst amount per 1 cm^2 of the IR cross-section.

3. Results and Discussion

An earlier XRD study [16] revealed that the original gibbsite used for thermal activation was well crystallized and did not have any impurities. As a result of the CTA process, a diffuse "halo" appeared on the diffraction pattern of the activated product (CTA product) in the angular range 2θ = 20–40°, which testified to the presence of the X-ray amorphous phase; reflections from crystalline boehmite (γ-AlOOH), which formed during thermal activation in large particles of gibbsite, were observed as well as the peaks of the original incompletely decomposed gibbsite [31]. In the present study, the same CTA product was used for the synthesis of MgAl$_2$O$_4$ samples.

Powder diffraction patterns of the interaction products MgAl(1)-110 and MgAl(2)-110 dried at 110 °C (Figure 1) are similar. It should be noted that since the samples were not washed after the synthesis, lines from the initial Mg(NO$_3$)$_2$·6H$_2$O are observed in the diffraction patterns. These lines overlap with the reflections from boehmite and gibbsite, which initially were present in the CTA product, thus indicating that these phases do not interact with magnesium nitrate in the samples in our experiment conditions. In addition, the diffraction patterns contain the reflections that are typical of layered double hydroxides (LDH), as shown in Figure 1A.

Figure 1B displays the diffraction patterns of MgAl(1)-550 and MgAl(2)-550 samples after thermal treatment at 550 °C. One can see the reflections that correspond to highly dispersed magnesium aluminate and MgO (diffraction pattern 1) or solely to highly dispersed MgAl$_2$O$_4$ (diffraction pattern 2). The size of the coherent scattering region of the MgO phase in the MgAl(1)-550 sample was ~90 Å, and for aluminates, nearly ~70 Å. According to the stoichiometry and quantitative analysis by atomic emission spectroscopy, each of the samples contain the same amount of magnesium, 17%. This suggests that the hydrothermal treatment provides a better mutual distribution of reagents, which results in the formation of single-phase aluminate despite the presence of gibbsite and boehmite impurities in this sample before thermal treatment.
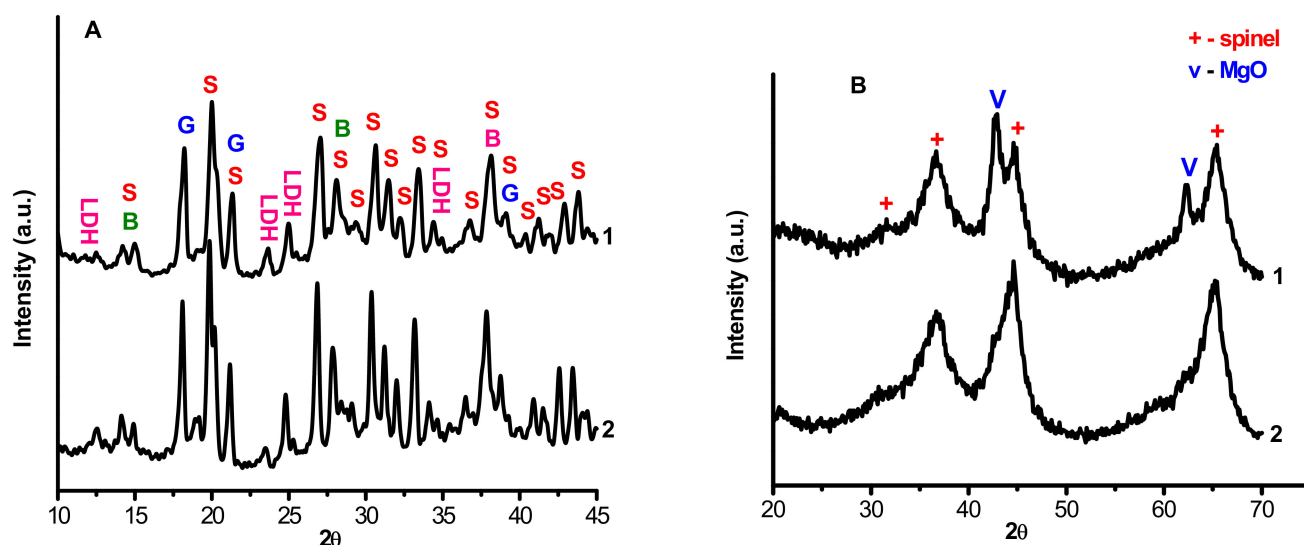
Figure 1. Powder diffraction patterns of the samples before (**A**) and after (**B**) calcination: 1—MgAl(1)-110 and MgAl(1)-550; 2—MgAl(2)-110 and MgAl(2)-550; S—$Mg(NO_3)_2 \cdot 6H_2O$; G—gibbsite; B—boehmite; LDH—double hydroxide.

It should be noted that the obtained samples of magnesium aluminate $MgAl_2O_4$ have different values of lattice parameters. The sample synthesized under hydrothermal conditions has the lattice parameter $a = 8.093$ Å, which slightly exceeds the tabular value for the high-temperature $MgAl_2O_4$ ($a = 8.080$ Å, PDF no. 21-1152), whereas the lattice parameter a for the $MgAl_2O_4$ synthesized under mild conditions is close to the tabular value and equal to 8.084 Å. A higher value of the lattice parameter for MgAl(2)-550 may testify to its anionic modification.

According to thermal analysis data, the original gibbsite is characterized by a total weight loss of ~34% and the presence of endothermic effects: the endo-effect at 97 °C caused by the removal of weakly bound molecular water; the double pre-effect with the maxima at 238 and 256 °C indicates the initial decomposition step of plate-like gibbsite crystallites with the formation of boehmite, the main endothermic effect produced by dehydration of the gibbsite phase (the peak at 314 °C), and the endo-effect resulting from decomposition of the boehmite phase at 536 °C. Thermal activation of gibbsite leads to a decrease in the weight loss up to ~12.5%. The endothermic effect with the maximum at 103 °C appears on the TA curve of the CTA product of gibbsite; this effect is caused by the removal of molecular water from the X-ray amorphous alumina component of the product [31]. Along with this, two effects are retained: the endo-effect caused by dehydration of the residual gibbsite phase to χ-Al_2O_3 with the extremum at 267 °C, and the endothermic effect at 495 °C related to decomposition of boehmite to γ-Al_2O_3. The presence of gibbsite and boehmite in the CTA product was revealed as well. According to the data reported in [23,25,30], the presence of an exothermic effect with the maximum at 800–850 °C in the CTA product of gibbsite testifies to the crystallization of the X-ray amorphous phase into a γ-like low-temperature Al_2O_3 species.

Thermograms were dried to a constant weight at 110 °C and products of the interaction of MgAl(1)-110 and MgAl(2)-110, which were obtained under mild and hydrothermal conditions, are displayed in Figure 2A,B. They essentially differ from the thermogram of the CTA product of gibbsite. These differences are caused by an increase in weight losses from 12.5 [31] to ~56–58% and by the appearance of new thermal effects indicating the formation of mixed double hydroxides. It is known that the heating curves of layered double hydroxides commonly have three weight loss regions that are caused by gradual dehydroxylation of the layered structure: the low-temperature region (up to 150 °C) corresponds to the removal of physisorbed water; in the temperature range of 200–300 °C the removal of interlayer water takes place; and in the region of 350–500 °C, the brucite-like

layers are dehydroxylated and interlayer anions $(A)^{n-}$ are removed [1,2,6]. Thermograms of MgAl(1)-110 and MgAl(2)-110 samples contain the following thermal effects: in the temperature region of 62–133 and 90–110 °C, weakly bound molecular water is removed; endo-effects at 197 and 189 °C are related to the beginning of the removal of interlayer water from the structure of double hydroxides; effects with the extremums at 305 and 306 °C, which are observed for both samples, are caused by dehydration of gibbsite that is present in the CTA product of gibbsite before its treatment in $Mg(NO_3)_2$ solutions (Figure 3B); and identical endothermic effects for both samples with the minima at ~356, 421 and 404 °C correspond to the final dehydroxylation of brucite-like layers and the removal of interlayer NO_3^- anions in Mg-Al double hydroxides [1,2]. The endo-effect with the maximum at 485 °C is caused by the decomposition of boehmite, which is present in the initial CTA product of gibbsite. The disappearance of the exo-effect at 826 °C testifies to the interaction of the X-ray amorphous component of the initial CTA product of gibbsite with water and magnesium aqua-complexes, which provides the formation of layered double hydroxides. The data obtained are consistent with the results of X-ray analysis, evidencing the formation of double hydroxides in the interaction products and termination of their thermal decomposition at 500–550 °C. It is known that magnesium–aluminum double hydroxides are layered compounds of a variable composition, such as hydrotalcite of the general formula $[Mg_{1-x}Al_x(OH)_2]^{x+}(NO_3) \cdot mH_2O$, formed by positively charged hydroxide layers $[Mg_{1-x}Al_x(OH)_2]^{x+}$, labile anions (nitrates in our case) and water molecules located in the interlayer space. The formal equation for the formation of double hydroxide from the reagents used can be represented by the following scheme:
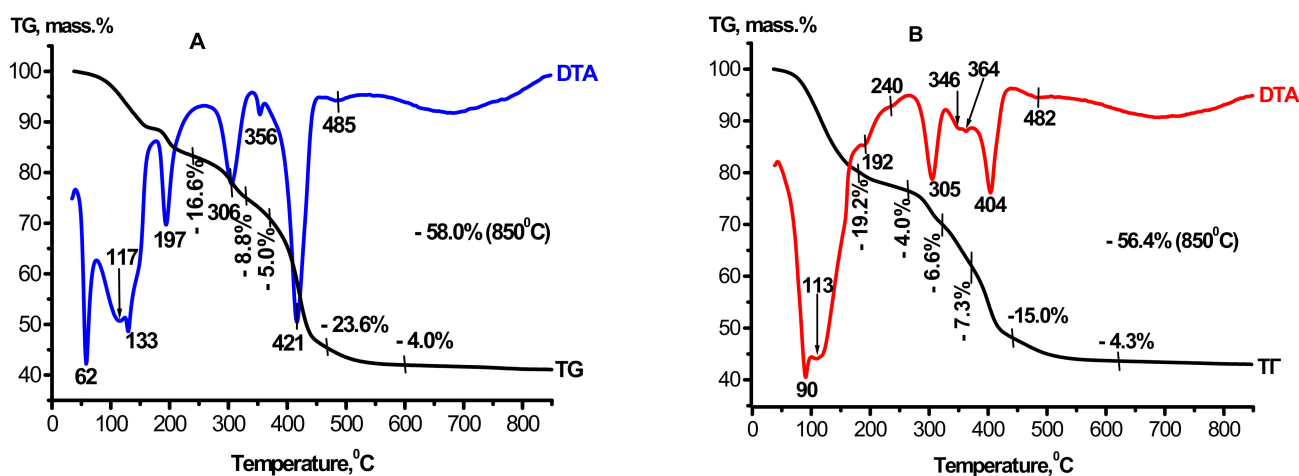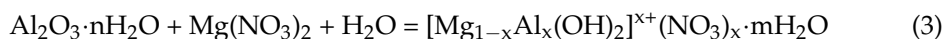
$$Al_2O_3 \cdot nH_2O + Mg(NO_3)_2 + H_2O = [Mg_{1-x}Al_x(OH)_2]^{x+}(NO_3)_x \cdot mH_2O \qquad (3)$$

Figure 2. Data on thermal analysis of the samples: (**A**)—MgAl(1)-110; (**B**)—MgAl(2)-110. The graphs have been changed a bit.

According to the electron microscopy analysis, the MgAl(2)-550 sample obtained by hydrothermal treatment and calcined at 550 °C consists mostly of 10–15 μm particles and a small amount of 30–40 μm particles. The elemental composition of different surface regions of this sample was analyzed by energy-dispersive X-ray spectroscopy at a probe electron energy up to 25 keV, which corresponds to the depth of the analyzed layer up to 5 μm. The analysis revealed the nearly uniform distribution of magnesium with an average weight ratio of Al/Mg = 2.26, which corresponds to the stoichiometric Al/Mg ratio in $MgAl_2O_4$. It was shown that the surface morphology of MgAl(2)-550 particles is formed by elongated needle-like particles (Figure 3D), which are typical of the spinels obtained by precipitation of double hydroxides [8].
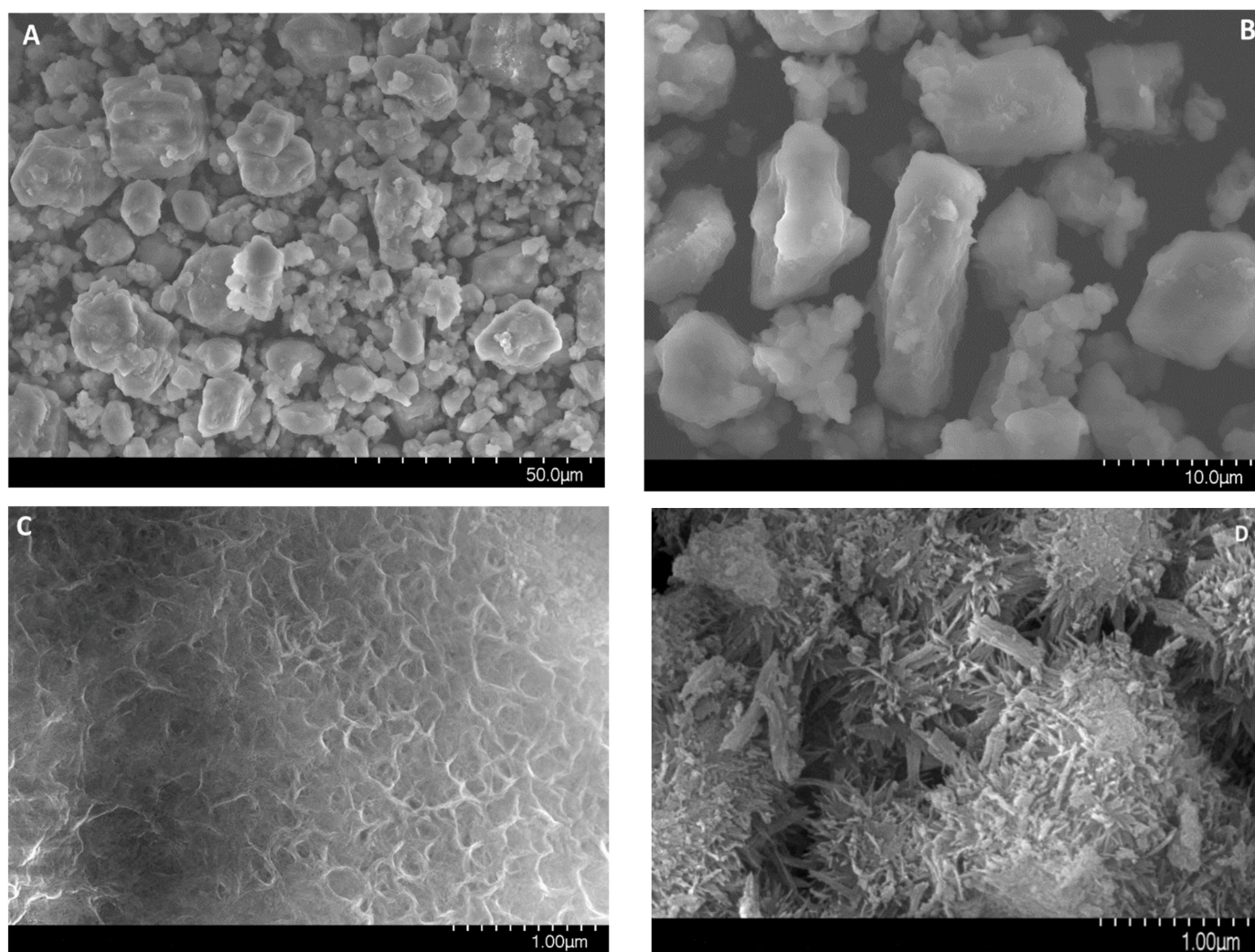
Figure 3. Electron microscopy images of MgAl(1)-550 (**A–C**) and MgAl(2)-550 (**D**) samples.

Electron microscopy images in Figure 3A–C demonstrate the formation of spherical aggregates with a size from 2 to 40 μm in the tested MgAl(1)-550 sample. Morphological differences between the samples are related to the texture of aggregates. Aggregates in the MgAl(2)-550 sample are made of needle-like particles, as in Figure 3D, whereas in the MgAl(1)-550 sample, the needle-like particles are observed only on the surface and their diversity is much smaller than in the MgAl(2)-550 sample, as in Figure 3B. In addition, according to the elemental composition identified by energy-dispersive X-ray spectroscopy at a probe electron energy up to 25 keV for different regions of MgAl(1)-550 particles, the average weight ratio of Al/Mg was ca. 3.5, which exceeds the stoichiometric ratio typical of spinel and testifies to a lower content of magnesium in the subsurface layer of particles in this sample. Since the presence of a magnesium oxide phase is observed in the sample, it can be represented by individual particles. The obtained quantitative data on the total magnesium content and Al/Mg weight ratio, as well as the XRD data, give grounds to estimate the total content of magnesium oxide phase in the MgAl(1)-550 sample as ca. 10 wt.%.

Figure 4 and Table 1 present textural characteristics obtained by nitrogen porosimetry for the alumina-magnesia samples calcined at 550 °C. The samples have a high specific surface area, above 100 m²/g. This indicates that the observed micron-level particles are porous and that the surface area consists mostly of the inner surface of the pores. The analysis of the obtained nitrogen adsorption isotherms shows that in all cases, the samples have a broad pore size distribution, from 3 to 200 nm. Therewith, the MgAl(2)-550 sample contains a greater amount of large pores as compared to MgAl(1)-550, which may be caused by textural differences in the tested samples, namely: in the case of MgAl(1)-550 (Figure 4A,B), the shape and size of the micron-level particles are close to the initial CTA product of gibbsite, while in the case of MgAl(2)-550 (Figure 3C,D), aggregates of needle-like particles are formed. Investigation of the samples by mercury porosimetry revealed the presence of even larger pores, as shown in Figure 4B. For the MgAl(1)-550 sample, two maxima are observed at 1 and 11 μm (Figure 4B (1)) while for MgAl(2)-550, these maxima have a higher intensity and are shifted toward greater pore sizes of up to 11 and 20 μm (Figure 4B (2)). The data obtained indicate a somewhat larger average size of the micron-level particles detected by electron microscopy, which form large pores in the case of MgAl(2)-550. Since the pore surface area estimated from the mercury porosimetry data is approximately two times smaller than the value obtained from nitrogen desorption due to inaccessibility of small pores to porosimetry, it can be concluded that the narrowest pores make a significant contribution (~50%) to the specific surface area of MgAl(1)-550.
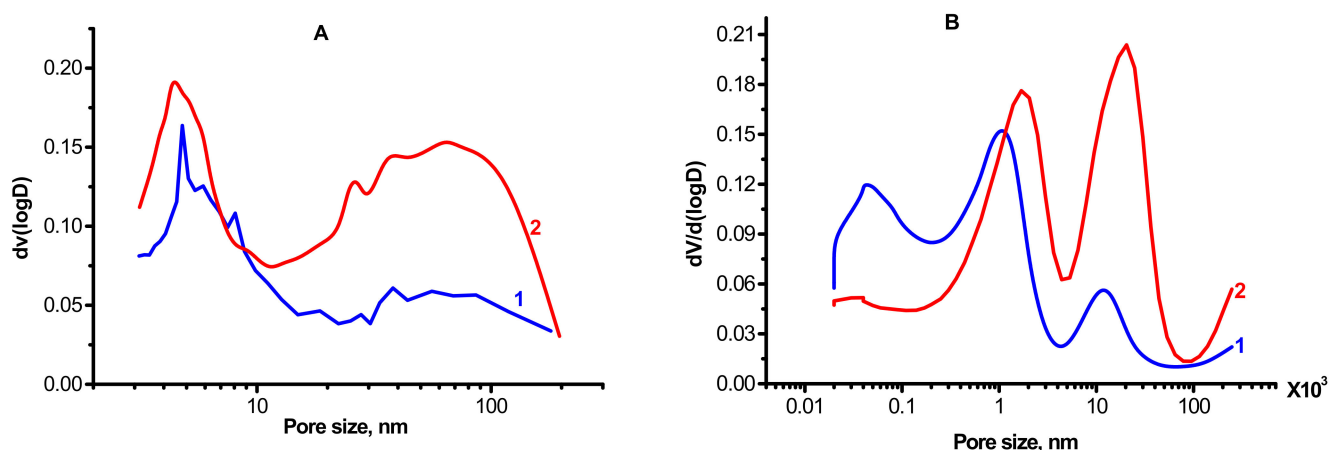

Figure 4. Nitrogen (**A**) and mercury (**B**) porosimetry curves of the samples: 1—MgAl(1)-550; 2—MgAl(2)-550.

Table 1. Textural characteristics of the samples.

Sample	Nitrogen Porosimetry Data			Mercury Porosimetry Data		
	S_{sp}, m²/g	Mean Pore Diameter, nm	Pore Volume, mL/g	S_{sp}, m²/g	Mean Pore Diameter, nm	Pore Volume, mL/g
MgAl(1)-550	102	4.0	0.13	39	277	0.32
MgAl(2)-550	150	3.8	0.21	71	1460	0.44

Thus, the synthesized samples have a hierarchical pore structure formed by the micron-level particles of different sizes (1–2 and 10–20 μm) consisting of ~70 nm crystallites that contain ~3 nm pores; the samples differ primarily in the total pore volume and quantitative ratio of the pores (Table 1).

Figure 5 displays the IR spectra of adsorbed CO on alumina-magnesia systems recorded with a pressure variation from 0.1 to 10 Torr. According to the spectra, MgAl(1)-550 and MgAl(2)-550 samples obtained by hydration at room temperature and hydrothermal treatment, respectively, contain similar types of LAS, which are characterized by an absorption band (a.b.) of adsorbed CO at 2153–2154, 2163–2165 and 2187–2188 cm^{-1}. The first absorption band is caused by CO adsorption on OH groups and Mg^{2+} cations [32], while in the individual modifications of Al$_2$O$_3$, only by CO adsorption on OH groups [19]. The absorption bands at 2163–2165 cm^{-1} are caused by CO adsorption on Mg^{2+} cations, which are the representatives of weak LAS. Lewis acid sites—the Al^{3+} cations in MgAl(1)-550 and MgAl(2)-550—are characterized by a.b. at 2187–2188 cm^{-1} and have a moderate strength [32]. Thermal treatment of MgAl(1)-850 and MgAl(2)-850 samples at 850 °C leads to a considerable decrease in the a.b. intensities in the region of adsorbed CO, which testifies to a decrease in their amount (Figure 5b,d). In addition, this is accompanied by the disappearance of a.b. at 2187–2188 cm^{-1}, corresponding to the LAS of moderate strength. As a result, the surface of MgAl(1)-850 and MgAl(2)-850 samples after calcination at 850 °C is characterized by the presence of only weak LAS with a.b. at 2170 cm^{-1}, which is simultaneously associated with CO adsorption on both the Mg^{2+} and Al^{3+} cations. As in the case of MgAl(1)-550 and MgAl(2)-550 samples (Figure 5a,c), the absorption bands at 2148–2151 cm^{-1} (Figure 5b,d) testify to the presence of adsorbed CO molecules on OH groups and magnesium ions.

IR spectroscopic studies of the acidity of alumina-magnesia samples were synthesized using the product of centrifugal thermal activation, showing that, irrespective of strongly differing treatment conditions of the CTA product in aqueous solutions of Mg(NO$_3$)$_2$, the samples after thermal treatment at 550 °C have an LAS of a close strength. Thus, MgAl(1)-550 and MgAl(2)-550 samples contain low and moderate strength LAS. However, the samples essentially differ in the amount of such sites, which is caused not only by different specific surface areas of the samples, but also by the density of sites (Table 2). The LAS concentration is lower for the mild hydration sample (MgAl(1)-550) than for the MgAl(2)-550 sample (Table 2). Since, according to the EDX data, the MgAl(1)-550 sample is characterized by an increased content of aluminum in the subsurface layer, this indicates that the surface of this sample is enriched in magnesium, apparently in the form of MgO, in contrast to the MgAl(2)-550 sample with stoichiometric, according to the EDX ratio of cations.

Elevation of the thermal treatment temperature to 850 °C provides a decrease not only in the LAS amount, which is disproportional to changes in their specific surface area, but also in the strength of LAS, which testifies to changes in the surface acidic properties of the oxides. MgAl(1)-850 and MgAl(2)-850 samples contain only weak LAS, which are characterized by the band of adsorbed CO with the maximum at 2170 cm^{-1}; therewith, the concentration of the indicated LAS types is much higher for the MgAl(2)-850 sample obtained by hydrothermal treatment (Table 2). Thus, a decrease in the LAS amount upon elevation of the treatment temperature is more pronounced for the mild hydration sample. This may be caused by an equalization of the magnesium oxide distribution over the surface of particles in the sample due to intensification of diffusion processes upon elevation of the sintering temperature, which increases the blocking of LAS.

A comparison of the obtained data on LAS characteristics with the well-known literature data on individual oxides of aluminum shows a much lower surface acidity (according to the strength and amount of LAS) of the synthesized MgAl(1)-550, MgAl(2)-550, MgAl(1)-850 and MgAl(2)-850 samples. In addition, the synthesized samples have a lower surface acidity also in comparison with the sample prepared by co-precipitation (Table 2 [33]). This may be related to the surface enrichment with magnesium cations of the samples synthesized in our study, which is more pronounced for MgAl(1)-T samples.
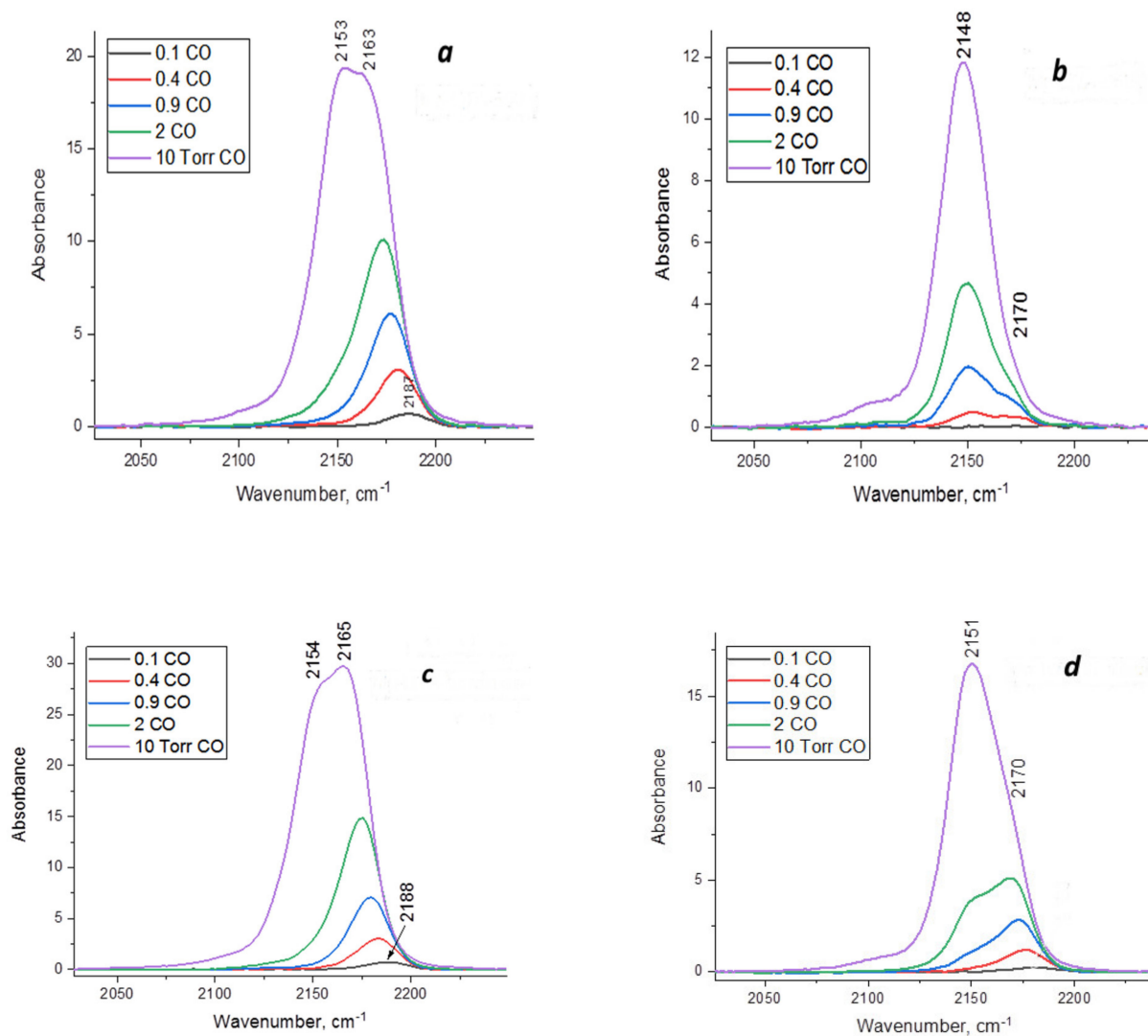
Figure 5. IR spectra of adsorbed CO on alumina-magnesia samples at 77 K and pressure in the range of 0.1–10 Torr: (**a**)—MgAl(1)-550; (**b**)—MgAl(1)-850; (**c**)—MgAl(2)-550; (**d**)—MgAl(2)-850.

Table 2. Characteristics of Lewis acid sites revealed by IR spectroscopy of adsorbed CO.

Sample	ν_{CO}, cm^{-1}	[LAS], µmol/g (µmol/m^2)	$\sum$[LAS], µmol/g (µmol/m^2)	Q_{CO}, kJ/mol	S_{sp}, m^2/g (BET)
MgAl(1)-550	2163–2187	304 (2.98)	304 (2.98)	21–33	102
MgAl(1)-850	2170	39 (0.52)	39 (0.52)	24	75
MgAl(2)-550	2165–2188	503 (3.35)	503 (3.35)	22–33	150
MgAl(2)-850	2170	161 (1.79)	161 (1.79)	24	90
Reference samples					
Al$_2$O$_3$ (CTA of gibbsite) [33]	2185–2200 2220 2235	932 19 17	968 (4.84)	31–39 49 56	200
γ-Al$_2$O$_3$ (precipitation) [33]	2185–2200	695	695 (2.44)	31–39	285
MgAl$_2$O$_4$ (precipitation) [8]	2163–2188	964	964 (6.6)	21–33	146

Thus, the distinctive feature of the samples synthesized in this work is an extremely low surface acidity in comparison not only with aluminum oxide but also with magnesium aluminate obtained by precipitation. In addition, it was shown that these properties can be changed in a wide range by varying the hydration conditions and calcination temperature, which opens new possibilities for controllable synthesis of the catalysts with desirable properties.

4. Conclusions

It was shown that the interaction of the thermal activation product of gibbsite with a magnesium nitrate solution under mild and hydrothermal conditions results in the formation of the layered double hydroxide phase. Thermal treatment of the interaction products at 550 °C leads to highly dispersed magnesium aluminate phases with the specific surface area above 100 m^2/g, which differ in the lattice parameter, texture, composition and acidity of the surface.

Depending on the synthesis conditions, the magnesium aluminate samples obtained in the study have a much smaller amount of Lewis acid sites and their concentration on the surface in comparison not only with aluminum oxides, but also with magnesium aluminate prepared by precipitation.

The study demonstrates that it is possible to obtain highly dispersed magnesium aluminate with a variable texture and a decreased surface acidity; the acidity can be finely adjusted by varying the synthesis conditions, which is of particular interest when this material is produced for various applications. In comparison with the conventional precipitation method, the proposed synthesis method of magnesium aluminates makes it possible to considerably decrease the amount of initial reagents and the number of technological steps, and also to minimize or completely exclude the formation of wastewater.

Author Contributions: Conceptualization, methodology, A.V.Z. and V.Y.K.; investigation, T.S.G. and E.A.S.; data curation, writing—original draft preparation, L.A.I. All authors have read and agreed to the published version of the manuscript.

Data Availability Statement: Not applicable.

Conflicts of Interest: There is no conflict of interest exits in the submission of this manuscript.

References

1. Li, F.; Duan, X. Applications of layered double hydroxides. *Struct. Bond.* **2006**, *119*, 193–223. [CrossRef]
2. Gareth, R.; O'Hare, D. Towards understanding, control and application of layered double hydroxide chemistry. *J. Mat. Chem.* **2006**, *16*, 3065–3074. [CrossRef]
3. Pankina, G.B.; Chernavsky, P.A.; Lunin, V.V. Dynamics of hydrogenation for bimetallic Co-Fe/Carrier catalysts. *Russ. J. Phys. Chem. A.* **2013**, *87*, 1622–1626. [CrossRef]
4. Belskaya, O.B.; Stepanova, L.N.; Gulyaeva, T.I.; Golinskii, D.V.; Belyi, A.S.; Likholobov, V.A. Study of Pt/MgAlO$_x$ catalysts in n-decane dehydrogenation. *Kinet. Catal.* **2015**, *56*, 655–662. [CrossRef]
5. Thesis, F.L.; Ayoko, G.A.; Frost, R.L. Synthesis of layered double hydroxides containing Mg^{2+}, Zn^{2+}, Ca^{2+} and Al^{3+} layer cations by co-precipitation methods—A review. *Appl. Surf. Sci.* **2016**, *383*, 200–213. [CrossRef]
6. Bocanegra, S.A.; Ballarini, D.A.; Scelza, O.A.; de Miguel, S.R. The influence of the synthesis routes of MgAl$_2$O$_4$ on its properties and behavior as support of dehydrogenation catalysts. *Mat. Chem. Phys.* **2008**, *111*, 534–541. [CrossRef]
7. Othman, M.R.; Helwani, Z.; Martunus; Fernando, W.J.N. Synthetic hydrotalcites from different routes and their application as catalysts and gas adsorbents: A review. *App. Organ. Chem.* **2009**, *23*, 335–346. [CrossRef]
8. Korneeva, E.V.; Ivanova, A.S.; Bondareva, V.M.; Plysova, L.M.; Glazneva, T.S. Structural, textural and acid-base properties of layered Mg-Al oxides modified with a tungstate or phosphate and their activity and selectivity in gas-phase glycerol dehydration. *Kinet. Catal.* **2015**, *56*, 605–616. [CrossRef]
9. Liu, J.; Bing, W.; Xue, X.; Wang, F.; Wang, B.; He, S.; Zhang, Y.; Wei, M. Alkaline-assisted Ni nanocatalysts with largely enhanced low-temperature activity toward CO$_2$ methanation. *Catal. Sci. Techn.* **2016**, *6*, 3976–3983. [CrossRef]

10. Vols, P.; Hilbert, S.; Storr, B.; Bette, N.; Lißner, A.; Seidel, J.; Mertens, F. Methanation of CO_2 and CO by (Ni,Mg,Al)-hydrotalcite-derived and related catalysts with varied magnesium and aluminum oxide contents. *Ind. Chem. Res.* **2021**, *60*, 5114–5123. [CrossRef]

11. Xiao, X.; Wang, J.; Li, J.; Dai, H.; Jing, F.; Liu, Y.; Chu, W. Enhanced low-temperature catalytic performance in CO_2 hydrogenation over Mn-promoted NiMgAl catalysts derived from quaternary hydrotalcite-like compounds. *Int. J. Hydrogen Energy* **2021**. [CrossRef]

12. Trukhanov, A.V.; Astapovich, K.A.; Turchenko, V.A.; Almessiere, M.A.; Slimani, Y.; Baykal, A.; Sombra, A.S.B.; Zhou, D.; Jotania, R.B.; Singh, C.; et al. Influence of the dysprosium ions on structure, magnetic characteristics and origin of the reflection losses in the Ni-Co spinels. *J. Alloys Compd.* **2020**, *841*, 155667. [CrossRef]

13. Algarou, N.A.; Slimani, Y.; Almessiere, M.A.; Alahmari, F.S.; Vakhitov, M.G.; Klygach, D.S.; Trukhanov, S.V.; Trukhanov, A.V.; Baykal, A. Magnetic and microwave properties of $SrFe_{12}O_{19}/MCe_{0.04}Fe_{1.96}O_4$ (M = Cu, Ni, Mn, Co and Zn) hard/soft nanocomposites. *J. Mater. Res. Technol.* **2020**, *9*, 5858–5870. [CrossRef]

14. Almessiere, M.A.; Güner, S.; Slimani, Y.; Hassan, M.; Baykal, A.; Gondal, M.A.; Baig, U.; Trukhanov, S.V.; Trukhanov, A.V. Structural and magnetic properties of $Co_{0.5}Ni_{0.5}Ga_{0.01}Gd_{0.01}Fe_{1.98}O_4/ZnFe_2O_4$ spinel ferrite nanocomposites: Comparative study between sol-gel and pulsed laser ablation in liquid approaches. *Nanomaterials* **2021**, *11*, 2461. [CrossRef]

15. Algarou, N.A.; Slimani, Y.; Almessiere, M.A.; Sadaqat, A.; Trukhanov, A.V.; Gondal, M.A.; Hakeem, A.S.; Trukhanov, S.V.; Vakhitov, M.G.; Klygach, D.S.; et al. Functional $Sr_{0.5}Ba_{0.5}Sm_{0.02}Fe_{11.98}O_4/x(Ni_{0.8}Zn_{0.2}Fe_2O_4)$ hard-soft ferrite nanocomposites: Structure, magnetic and microwave properties. *Nanomaterials* **2020**, *10*, 2134. [CrossRef]

16. Bocanegra, S.A.; Guerrero-Ruiz, A.; Scelza, O.A.; de Miguel, S.R. $MgAl_2O_4$ spinel prepared by mechanochemical synthesis used as a support of multimetallic catalysts for paraffin dehydrogenation. *Catal. Ind.* **2013**, *5*, 61–73. [CrossRef]

17. Karagedov, G.R. Mechanochemically stimulated synthesis and low temperature sintering of $MgAl_2O_4$. *Chem. Sus. Dev.* **2020**. [CrossRef]

18. Stepanova, L.N.; Kobzar, E.O.; Leont'eva, N.N.; Belskaya, O.B. Study of the Mg (Li, Co, Ni) Al-LDH prepared by mechanochemical route during Pt(IV) chloride complexes adsorption. *AIP Conf. Proc.* **2020**, *2301*, 020003. [CrossRef]

19. Williams, G.R.; Moorhouse, S.J.; Prior, T.J.; Fogg, A.M.; Rees, N.H.; O'Hare, D. New insights into the intercalation chemistry of $Al(OH)_3$. *Dalton Trans.* **2011**, *40*, 6012–6022. [CrossRef]

20. Fogg, A.M.; Williams, G.R.; Chester, R.; O'Hare, D.A. Novel family of layered double hydroxides–$[MAl_4(OH)_{12}](NO_3)_2 \cdot xH_2O$ (M=Co, Ni, Cu, Zn). *J. Mater. Chem.* **2004**, *14*, 2369–2371. [CrossRef]

21. Komlev, A.A.; Gusarov, V.V. Mechanism of the nanocrystals formation of the spinel structure in the $MgO-Al_2O_3-H_2O$ system under hydrothermal conditions. *Russ. J. Gen. Chem.* **2011**, *81*, 2222–2230. [CrossRef]

22. Lippens, B.C.; Steggerda, J.J. *Physical and Chemical Aspects of Adsorbents and Catalysts*; Linsen, B.G., Ed.; Academic Press: London, UK, 1970; p. 232.

23. Tanashev, Y.Y.; Moroz, E.M.; Isupova, L.A.; Ivanova, A.S.; Litvak, G.S.; Amosov, Y.I.; Rudina, N.A.; Shmakov, A.N.; Stepanov, A.G.; Kharina, I.V.; et al. Synthesis of aluminum oxides from the products of the rapid thermal decomposition of hydrargillite in a centrifugal flash reactor. Physicochemical properties of the products obtained by the centrifugal thermal activation of hydrargillite. *Kinet. Catal.* **2007**, *48*, 153–161. [CrossRef]

24. Buyanov, R.A.; Krivoruchko, O.P.; Zolotovskii, B.P. On the nature of thermochemical activation of crystalline hydroxides. *Izv. Sib. Otdel. Akad. Nauk SSSR* **1986**, *1*, 39–44.

25. Danilevich, V.V.; Isupova, L.A.; Danilova, I.G.; Zotov, R.A.; Ushakov, V.A. Characteristics optimization of activated alumina desiccants based on product of a centrifugal thermal activation of gibbsite. *Russ. J. Appl. Chem.* **2016**, *89*, 343–353. [CrossRef]

26. Ingram-Jones, V.J.; Davies, R.C.T.; Southern, J.C.; Salvador, S. Dehydroxylation sequences of gibbsite and boehmite: Study of differences between soak and flash calcinations and of particle-size effects. *J. Mat. Chem.* **1996**, *6*, 73–79. [CrossRef]

27. Danilevich, V.V.; Klimov, O.V.; Nadeina, K.A.; Gerasimov, E.Y.; Cherepanova, S.V.; Vatutina, Y.V.; Noskov, A.S. Novel eco-friendly method for preparation of mesoporous alumina from the product of rapid thermal treatment of gibbsite. *Superlattices Microstruct.* **2018**, *120*, 148–160. [CrossRef]

28. Stolyrova, E.A.; Danilevich, V.V.; Klimov, O.V.; Gerasimov, E.Y.; Ushakov, V.A.; Chetyrin, I.A.; Lushchikova, A.E.; Saiko, A.V.; Kondrashev, D.O.; Kleimenov, A.V.; et al. Comparison of alumina supports and catalytic activity $CoMoP/\gamma$-Al_2O_3 hydrotreating catalysts obtained using flash calcination of gibbsite and precipitation method. *Catal. Today* **2020**, *353*, 88–98. [CrossRef]

29. Danilevich, V.V.; Isupova, L.A.; Parmon, V.N. The process for preparation of active aluminum hydroxyoxide via flash calcination of gibbsite in a new energy-efficient centrifugal drum-type reactor. *Clean. Eng. Techn.* **2021**, *3*, 100118. [CrossRef]

30. Isupova, L.A.; Kovalenko, O.N.; Andreeva, A.V.; Vedernikov, O.S.; Lamberov, A.A.; Pimerzin, A.A.; Reznichenko, I.D.; Tyshchenko, V.A.; Kleymenov, A.V.; Parmon, V.N. Aluminum oxide catalysts and supports obtained by thermal activation. *Katal. Prom.* **2021**, *21*, 368–381. [CrossRef]

31. Zhuzhgov, A.V.; Kruglykov, V.Y.; Suprun, E.A.; Protsenko, R.S.; Isupova, L.A. Synthesis of highly dispersed aluminum magnesium oxides from the product of centrifugal thermal activation of gibbsite. *Russ. J. App. Chem.* **2021**, *94*, 152–161. [CrossRef]

32. Paukshtis, E.A.; Yurchenko, E.N. Study of the acid–Base properties of heterogeneous catalysts by infrared spectroscopy. *Rus. Chem. Rev.* **1983**, *52*, 242–258. [CrossRef]

33. Ivanova, A.S.; Kul'ko, E.V.; Klimov, O.V.; Bukhtiyarova, G.A.; Litvak, G.S.; Budneva, A.A.; Paukshtis, E.A.; Zyuzin, D.A.; Moroz, E.M.; Zaikovskii, V.I.; et al. Influence of the texture and acid-base properties of the alumina-containing support on the formation of Co(Ni)-Mo catalysts for deep hydrodesulfurization of the diesel fraction. *Kinet. Catal.* **2008**, *49*, 791–801. [CrossRef]